JOURNAL OF MATERIALS SCIENCE **40** (2005) 187–197

Fabrication and plastic deformation of Y-TZP/alumina nanocomposite ceramics containing oxynitride glass

R. CHAIM
Department of Materials Engineering, Technion-Israel Institute of Technology, Haifa 32000, Israel

A. GOLDSTEIN
Israel Institute of Ceramics and Silicates, Technion-Israel Institute of Technology, Haifa 32000, Israel

I. ELDROR, A. GURMAN
Metallurgy Group, Engineering Center, Israel Aircraft Industries Ltd., Ben-Gurion International Airport 70100, Israel

Dense yttria-stabilized tetragonal zirconia polycrystals (Y-TZP) +28 vol% alumina nanocomposite ceramics with and without 17 vol% oxynitride glass were fabricated at 1380°C using microwave sintering. The specimens were uniaxially compressed in the temperature range 1250 to 1400°C. Strain rates as high as 10^{-4} (s^{-1}) were measured at 1350°C and 90 MPa in the glass-free specimens with the stress exponent of 1.5. Similar strain rates were measured at lower compressive stresses in the counterpart glass-containing specimens. The stress exponent in the glass-containing specimens changed from 1.0 at 1250°C to 2.0 at higher temperatures. Dynamic grain growth of the alumina grains was inhibited in the presence of the oxynitride glass. Plastic deformation at lower temperatures in glass-containing alloy occurred by cooperative grain boundary sliding, aided by viscous flow of the grain boundary glassy phase. The changes in the deformation behavior at higher temperatures were related to crystallization of the glass and simultaneous plastic deformation by grain boundary sliding.

1. Introduction

Creep and superplastic behavior of the alumina toughened zirconia (ATZ) composites have been thouroughly investigated in the last two decades. Increasing additions of alumina were found to increase the creep resistance of the ceramic composite [1–3]. Additions of alumina to zirconia is aimed towards stabilization of the tetragonal phase microstrucure and to enhance sintering. However, the two-phase assemblage may cause different physical and chemical interactions as was experimentally observed [3–6]. High alumina contents were found to simultaneously increase the creep resistance and the room temperature toughness of the composite [7, 8]. Refinement of the grain size of both alumina and zirconia phases is expected to enhance the superplastic behavior as well as the strength and toughness. This has led to the development of nanocomposite ATZ's [9–12]. An addition of grain boundary glassy phase is targeted towards enhancing both densification and plastic deformation [13–16]. However, based on the mutual solubility of the ceramic and the glassy phase, opposite trends such as inhibited grain growth and high resistance to creep may also be observed. As was noted by Clarisse *et al.* [3], the plastic deformation behavior in ATZ is influenced by the alumina-zirconia interfaces. Therefore, control of these interfaces by addition of appropriate glassy phase may lead to change in the deformation behavior at high temperatures. The present paper describes the plastic deformation behavior of zirconia toughened alumina (ZTA) nanocomposites containing an oxynitride glass as a grain boundary phase. This glass was chosen to provide amorphous grain boundary phase at short durations during the plastic deformation; yet it may be crystallized at longer durations at high temperatures to improve the mechanical properties of the deformed article.

2. Experimental procedures

ZTA powders were prepared by mixing commercial nanocrystalline zirconia powder (Daiichi Kigenso, HSY-3U, 3 mol%Y_2O_3) with 28 vol% nanocrystalline alumina powder (Baikalox CR-30, 99.99%) using attrition milling in isopropyl alchohol for 1 h. The ultimate crystallite size was between 30 to 80 nm for the HSY and 50 nm in the case of alumina powder, albeit, with

similar specific surface area of 20 (m^2/g). The black oxynitride glass (designated as ON glass), that contained (wt%) 43 SiO_2, 11 Si_3N_4, 25 Al_2O_3, 18 MgO, and 3 BaO, was melted at ~1650°C within a Molybdenum crucible under N_2 overpressure and followed by rapid quenching. The glass shards were comminuted in steps with a final attrition milling stage. The present glass was chosen to provide amorphous grain boundary phase at short durations during the plastic deformation; yet it may be crystallized at longer durations at high temperatures to improve the mechanical properties of the deformed article. The glass-containing ZTA powders were prepared by mechanical mixing of the appropriate powders to yield the final composition of (Y-TZP+28 vol% Al_2O_3) + 17 vol% ON glass (thereafter: ATZ-ON). This was followed by attrition milling for 30 min using alumina balls. Glass-free samples (thereafter: ATZ) were also prepared as reference samples.

The dry powders were uniaxially compacted into disc pellets of 25 mm in diameter and 12 mm thick, followed by cold isostatic pressing at 250 MPa. The relative green density was measured through weighing to be ~55%, regardless of the pellet composition. The pellets were sintered for 30 min at the peak temperature using a susceptor assisted MW furnace (MMT 101 MW), following the procedure developed previously [17]. The relative densities of the sintered specimens were determined by the Archimedes method.

Rectangular bars of 3 × 3 × 4 mm^3 were cut and uniaxially compressed under the constant load regime in the range of 4 to 140 MPa, while measuring the specimen contraction within the accuracy of ±2 μm. The specimens were annealed for 1 h at the testing temperature for equilibration and the compression tests lasted between 1.5 to 4 h at the testing temperature. The compression tests were performed between 1250 and 1400°C under N_2 atmosphere, using the SiC pressing pads. All the specimens were plastically deformed without a brittle failure.

The specimen microstructure prior to and after the deformation was characterized using scanning electron microscopy (SEM XL30), and transmission electron microscopy (TEM 2000FX), combined with X-ray energy dispersive spectroscopy (EDS). The specimens for the microscopy observations were prepared by conventional techniques.

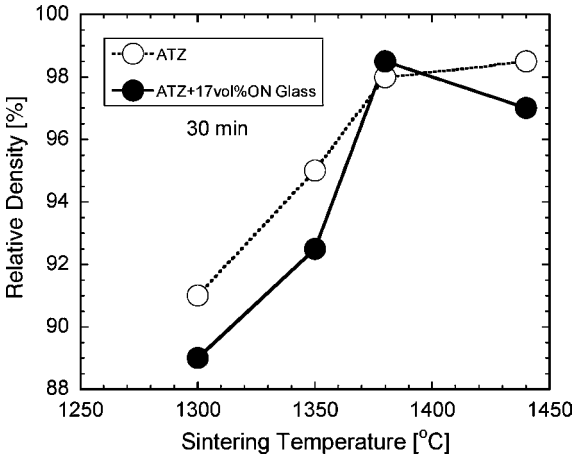

Figure 1 Relative density versus sintering temperature in the glass-free ATZ and ATZ containing oxynitride glass.

3. Results and discussion

3.1. Oxynitride glass

The nitrogen content of the glass was determined as ~2.5 wt%. The glass transition and melting temperatures were determined as 850 and 1390°C, respectively. It exhibited viscosity of 10^7 (Pa·s) at 1100°C. Chemical analysis has shown that the glass liquid dissolves up to 2 wt% ZrO_2 at 1300°C. In the powder form, this glass is prone to rapid crystallization at temperatures above 900°C. Nevertheless, no crystallization was observed in the nanocomposite specimens heat treated for short durations (below 2 h). At longer durations, crystallization occured at temperatures above 1280°C. Sessile drop tests have shown that above 1350°C full wetting of both the Y-TZP and Al_2O_3 substrates occurs by this oxynitride glass.

TABLE I Uniaxial deformation test conditions and results

No.	Composition	Deformation temp. (°C)	Deformation duration (h)	Total strain (%)	Grain size Y-TZP (μm)
1	Y-TZP+28 vol% Al	1275	3.7	68.0	
2	- : -	1300	2.85	72.5	
3	- : -	1300	2.85	[a]	
4	- : -	1325	3.0	52.5	
5	- : -	1325	3.2	65.5	
6	- : -	1350	3.5	51.5	0.31 ± 0.14
7	- : -	1350	2.5	41.7	
8	- : -	1375	2.1	58.0	0.50 ± 0.16
9	- : -	1400	1.35	31.7	
10	- : -	1400	1.35	52.5	0.53 ± 0.21
11	(Y-TZP+28 vol% Al) +17 vol% ON glass	1250	4.2	73.0	
12	- : -	1300	3.2	60.5	
13	- : -	1350	2.5	50.0	
14	- : -	1375	3.2	32.5	0.27 ± 0.25
15	- : -	1400	2.0	72.7	

[a]Exposed to high temperature without deformation.

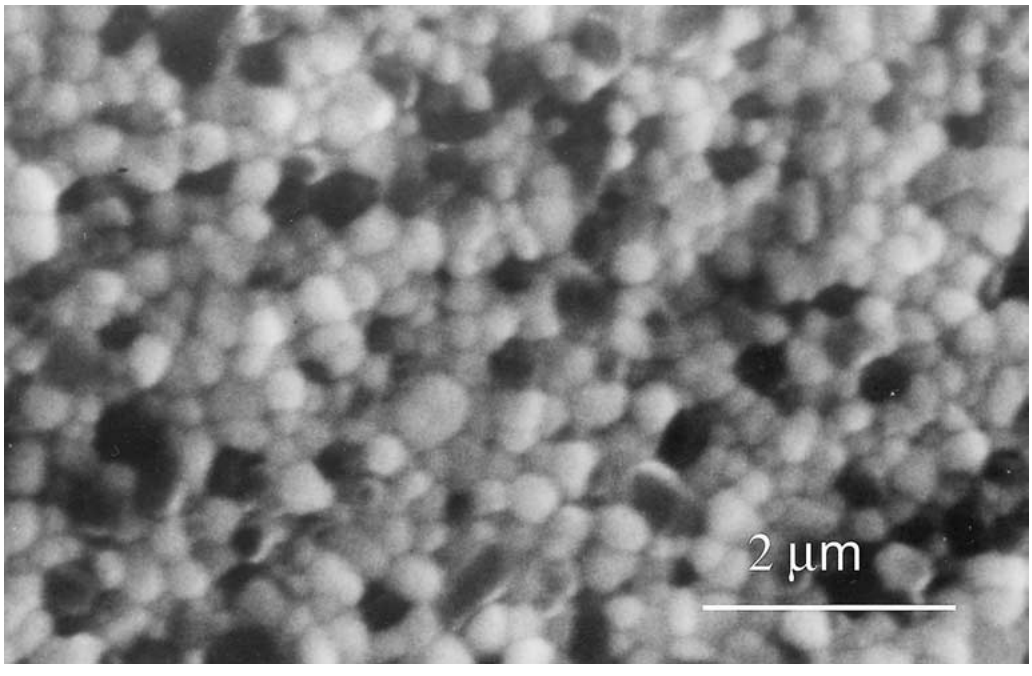

Figure 2 SEM image of the glass-free ATZ nanocomposite showing the homogeneous distribution of both alumina (dark) and zirconia (bright) grains.

3.2. Microwave sintering

The ATZ nanocomposites with and without the oxynitride glass were sintered using the MW heating aided by the SiC suceptors [17]. The change in the relative density of the two compositions versus the sintering temperature is shown in Fig. 1. At lower sintering temperatures, the glass-free (ATZ) samples exhibited higher densities compared to the glass-containing (ATZ-ON) samples. This effect is in agreement with the poor wetting ability of the glass on Y-TZP or alumina grains below 1350°C. At higher temperatures the ability of the liquid ON glass to wet and dissolve (to some extent) the matrix oxides enhances the densification via liquid phase sintering. Increasing the sintering temperature to 1440°C did not change significantly the final density of the ATZ samples. Nevertheless, some decrease in the density of the ATZ-ON sample was observed, and that may be related to bubble formation in the glassy phase and consequent pore retention within the sintered pellet. The sintered specimens contained the assemblage of stable alumina (corundum) and the tetragonal zirconia only, as was determined by the X-ray diffraction (not shown here). No monoclinic phase was detected. Therefore, a sintering temperature of 1380°C was selected for the fabrication of both dense and ultrafine grained samples. Microwave sintering at 1380°C for 30 min resulted in the average zirconia grain size of 250 and 450 nm in the glass-free and the glass-containing specimens, respectively. The zirconia grains exhibited a round-shape morphology in the ATZ-ON specimens (Fig. 2), indicating full wetting and some dissolution of the grains within the oxynitride glassy phase. The glassy phase at the grain boundaries and the triple junctions were found to be amorphous in the as-sintered specimens.

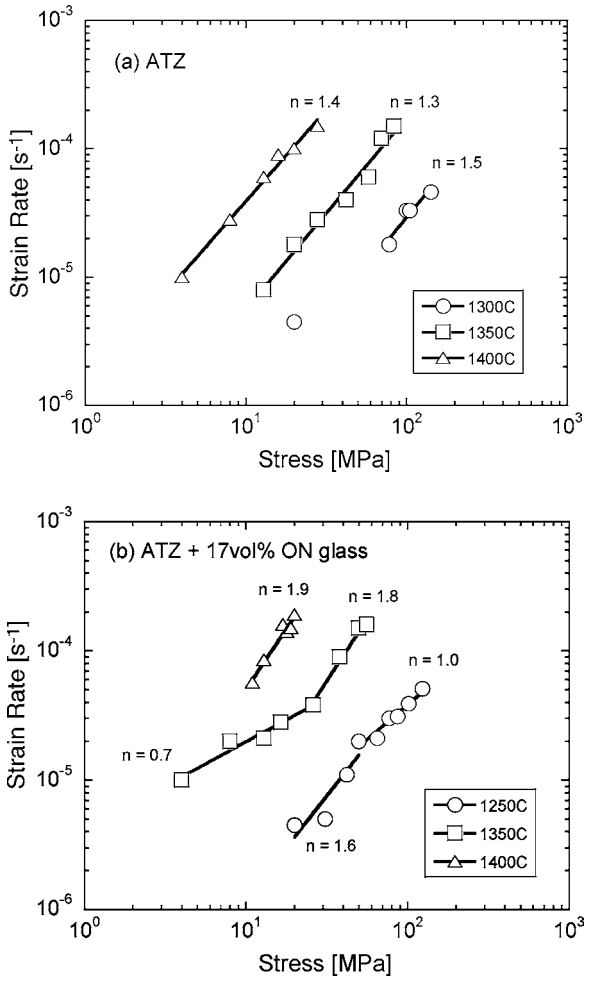

Figure 3 Strain rate versus compressive stress and temperature in glass-free ATZ and ATZ containing oxynitride glass.

3.3. Compression tests

The overall deformation conditions were summarized in Table I. For clarity, only the strain rate versus stress at the temperature range 1300 to 1400°C for ATZ specimens is shown in Fig. 3a. The strain rate increases

rapidly with stress and temperature. A temperature increase by 100°C leads to an increase by almost two orders of magnitude in the strain rate. Strain rates as high as 10^{-4} (s^{-1}) were recorded at 1350°C and 75 MPa. The stress exponent (slopes of the curves) varied between 1.4 to 1.6, exhibiting basically the average exponent of 1.5 compared to the average value of 2.0 that was found in many investigations for ATZ alloys with submicrometer grain size [18–22]. The stress exponents of 1.3 to 1.9 were reported by Wakai *et al.* [22] for the

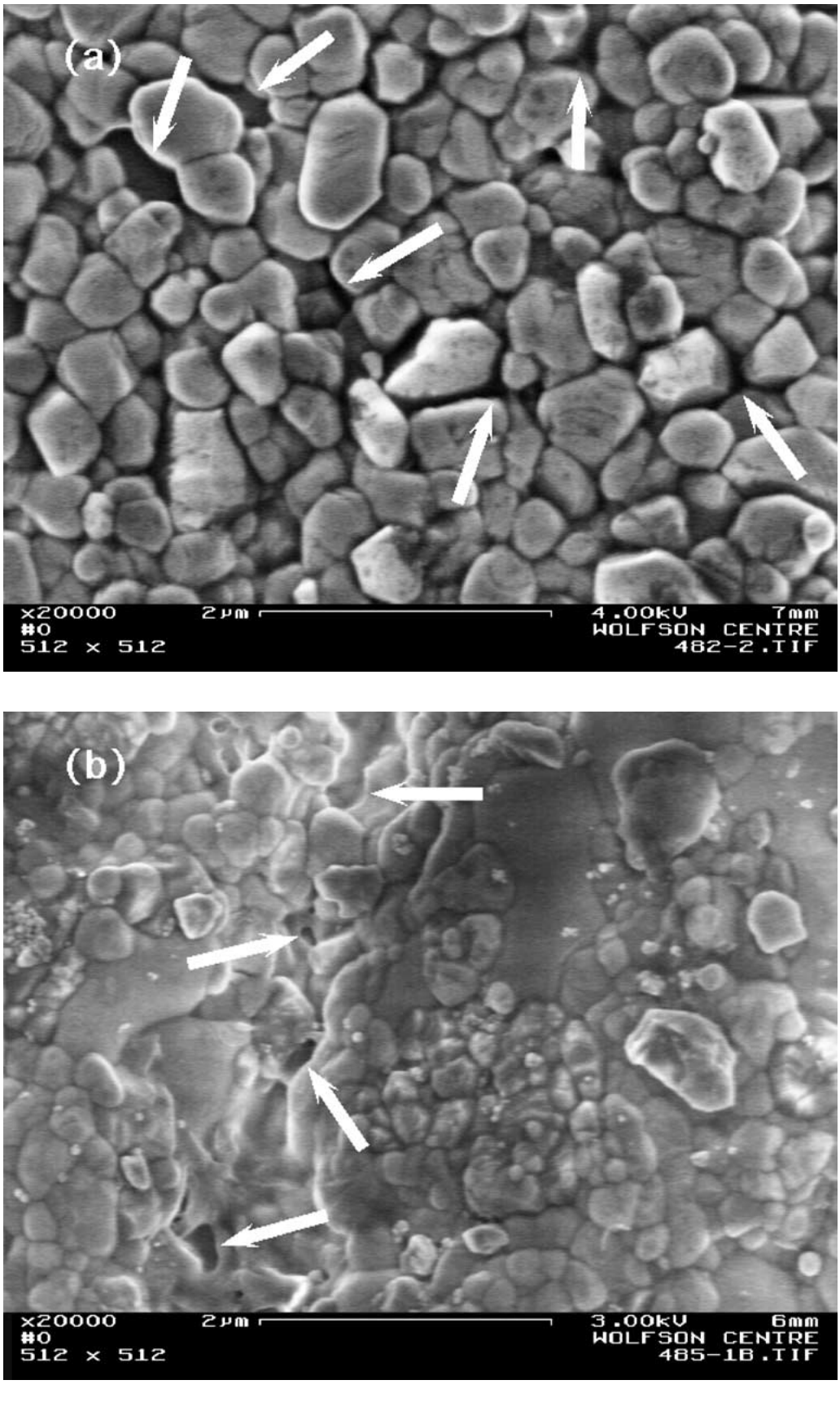

Figure 4 SEM image of the glass-free ATZ specimens deformed at different temperatures: (a) 1275°C for 3.7 h and 68% deformation and (b) 1400°C for 1.3 h and 52% deformation. The arrows point to the cavities.

present ATZ composition, tested by compression between 1400–1500°C. For comparison, the stress exponent value in the Y-TZP ceramics was reported in a wide range between 1.2 to 3.8, depending on the alloy compositional and microstructural characteristics, as well as on the stress level and other deformation conditions [23]. A similar plot for the ATZ-ON glass specimens is shown in Fig. 3b. Comparison between the strain rates in the ATZ (Fig. 3a) and the ATZ-ON glass (Fig. 3b) revealed that the similar strain rates in the latter were observed at lower stresses and lower temperatures. In addition, at the lowest deformation temperature (i.e.,

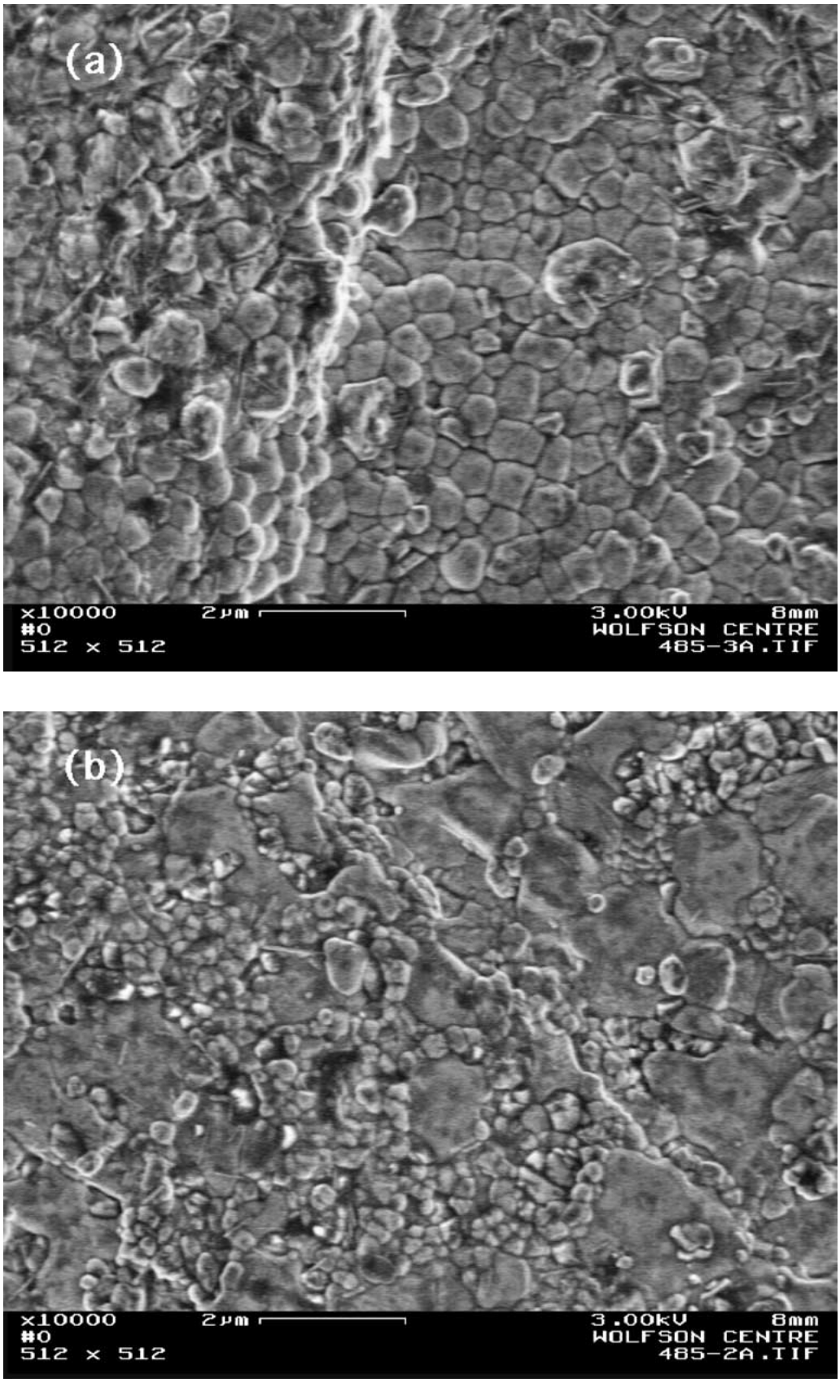

Figure 5 SEM image of the glass-free ATZ specimens: (a) Annealed at 1300°C for 2.8 h and (b) Deformed at 1300°C for 2.8 h and 72% deformation.

1250°C) the stress exponent decreased from 1.6 at low stresses to 1.0 at higher stresses. Nevertheless, the stress exponent was found to increase to $n = 2$ at the higher deformation temperatures. This may indicate a change in the deformation mechanism where stress exponents 2 and 1 imply grain boundary sliding and diffusional creep, respectively [24]. The exponent 1.0 at 1250°C may be related to viscous flow of the glassy phase, when

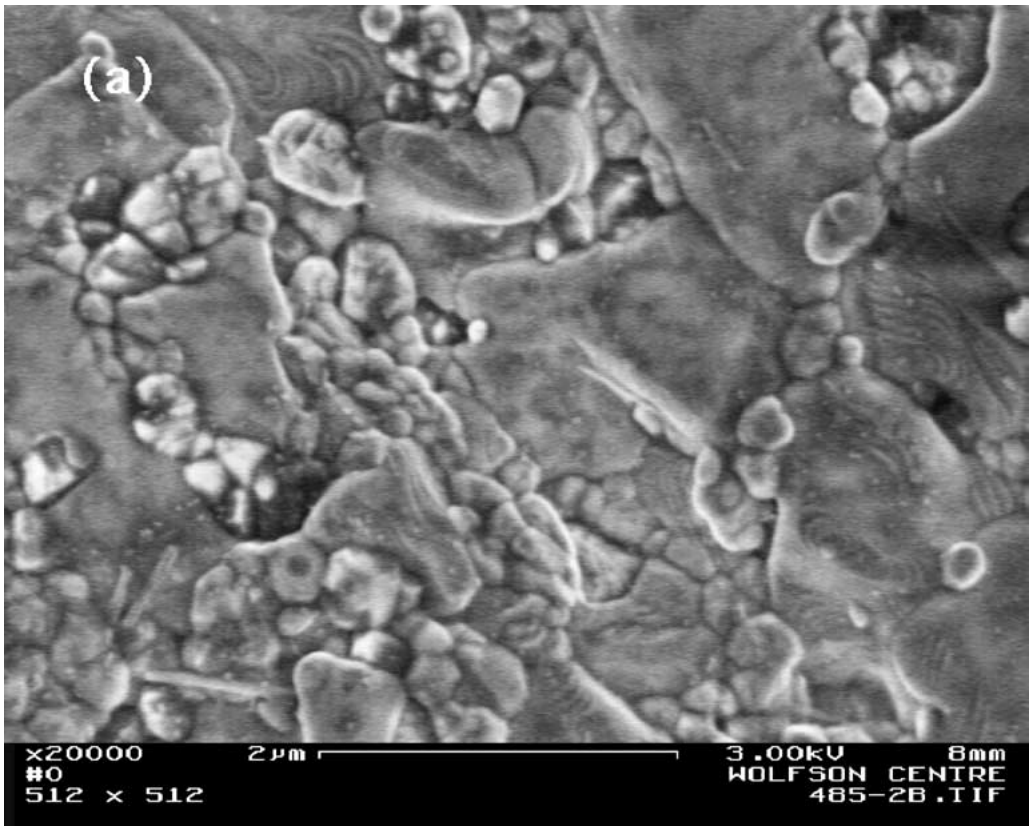

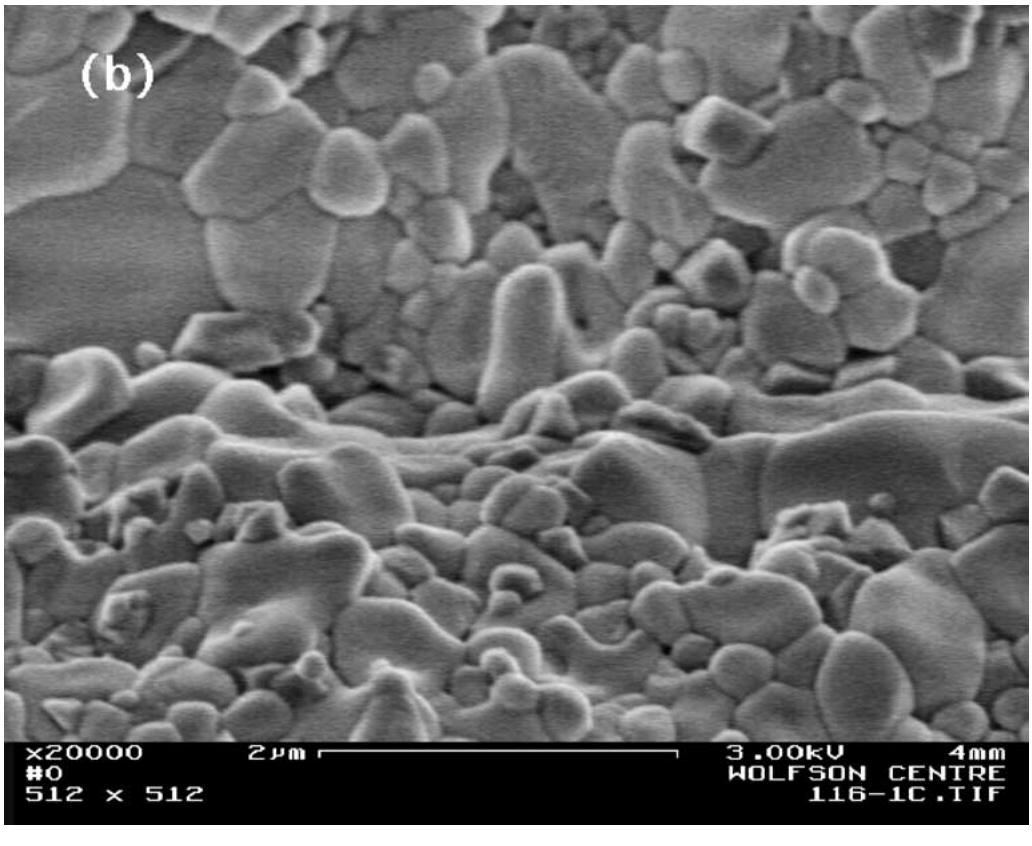

Figure 6 SEM images from the specimens deformed at 1300°C: (a) Glass-free ATZ with 72% deformation, (b) Glass-containing ATZ with 60% deformation. The enhanced dynamic grain growth of the alumina grains in (a) is apparent, and (c) Cooperative grain boundary sliding results to clusters of grains at the deformed surfaces. (*Continued*)

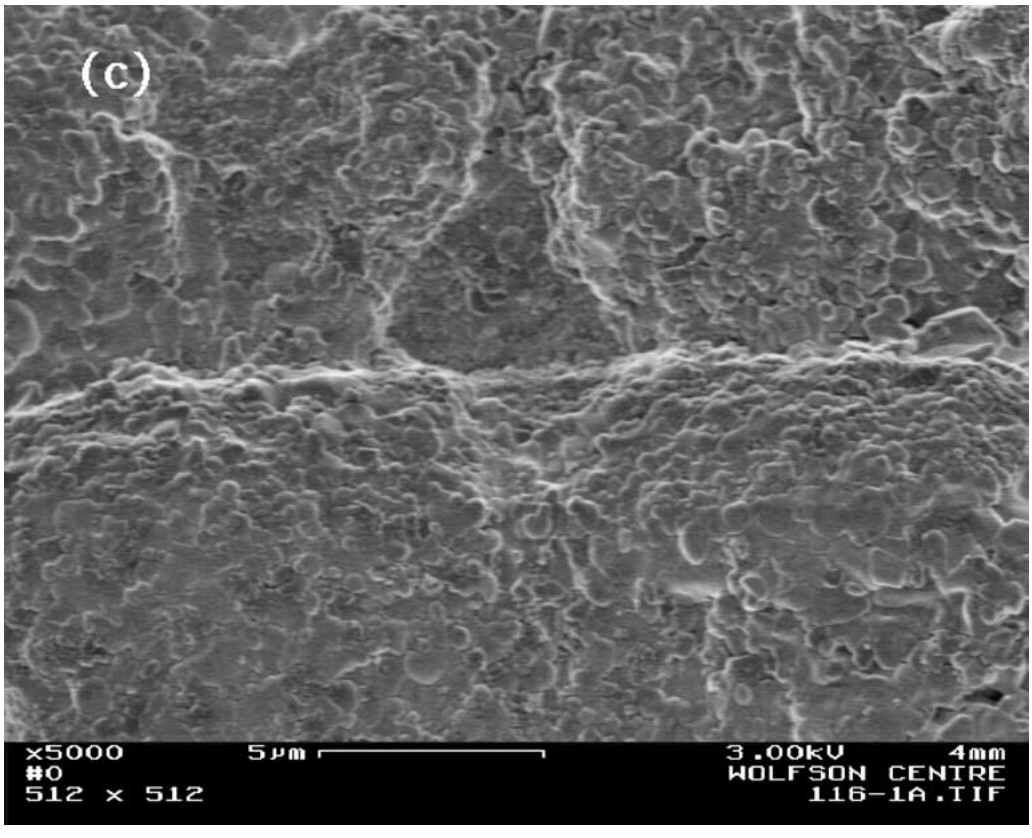

Figure 6 (*Continued*)

the threshold stress (i.e., 50 MPa) is reached. Although the high stress exponents at low stress regimes can be rationallized using the threshold stress approach [25], there is no theory that explains the stress exponents around 1.5.

3.4. Microstructure

The surface and the bulk microstructures of the specimens prior to and after the deformation were characterized using SEM and TEM, respectively. Both techniques have shown remarkable grain continuity within the different specimens subjected to more than 50% of the plastic deformation. SEM image of the glass-free ATZ specimen prior to the deformation is shown in Fig. 2. The submicron size of both alumina (dark grains) and zirconia (bright grains) as well as their homogeneous distribution is visible. SEM images of the glass-free ATZ specimens, deformed at different temperatures, are shown in Fig. 4. The sizes of both zirconia and alumina grains were kept in the submicron range at the lowest deformation temperature (i.e., 1275°C in Fig. 4a). Only a few randomly distributed cavities were observed at the surface (arrowed in Fig. 4a) after 68% of the plastic deformation. However, at the highest deformation temperature (i.e., 1400°C in Fig. 4b) significant growth of the alumina grains was observed. The Y-TZP grain size was yet in the submicron regime. The cavities at this temperature were relatively large with non-homogeneous distribution, indicating the local weakening of certain grain boundaries. The occurence of the cavities was more frequent at the alumina/Y-TZP than at the Y-TZP/Y-TZP grain boundaries.

The dynamic grain growth was found to be accelerated compared to the static grain growth, as shown in Fig. 5. SEM image of the glass-free ATZ specimen heat-treated only (Fig. 5a), adjacent to the similar specimen subjected to the compression test at 1300°C (Fig. 5b), has shown finer grain size of both zirconia and alumina phase in the former. This enhanced dynamic grain growth is in agreement with previous works [26]. The finer zirconia grains (see Table I) after deformation may be related to partition of the zirconia grains to subgrains aided by sintering stresses or applied load as is observed in the literature [27].

The glass addition to the present nanocomposite ATZ specimens had a twofold effect. First, the dynamic grain growth during the plastic deformation was retarded as demonstrated in Fig. 6. The grain growth in the glass-free specimen (Fig. 6a) may be associated with Ostwald ripening during which large alumina grains evolve but lead to finer zirconia grains [28]. This process is absent in the glass-containing specimens (Fig. 6b), where both alumina and zirconia grains grew to a much lower extent. The fact that, at the same time, oxynitride glass enhanced sintering and retarded grain growth may be explained as following. The presence of the glassy phase may enhance the densification via the liquid phase sintering. However, while dense, the grain shape is accommodated to its neighbor grains, resulting in grain boundaries with or without a glassy phase (depending on the grain orientation). The impurity atoms in the glass-free grain boundaries may only lower the grain boundary mobility compared to that of impurity-free boundary, where the glassy phase pockets (at triple junctions) may act as pinning point for the grain boundaries. However, the grain boundaries are faceted (i.e., flat curvature)

in the presence of the glassy phase, thus lacking the driving force for grain growth. Another effect of the glass is enhancement of the cooperative grain boundary sliding, as shown in Fig. 6c. This low magnification SEM image reveals the surface microstructure after the deformation. The surface is rumpled due to cooperative grain boundary sliding of the 5 to 10 micrometer grain clusters. Cooperative grain boundary sliding was clearly demonstrated in zirconia alloys with addition of glassy phases [29, 30], similar to deformation of glanular materials [31].

TEM observations were consistent with the microstructural findings in SEM. TEM images from the glass-free nanocomposite ATZ, deformed at 1375°C (Fig. 7a), have shown that the ultra-fine Y-TZP and the submicron size alumina grains were homogeneously distributed. Both phases exhibited faceted grain boundaries. Many of the Y-TZP grains were dislocated or internally twinned. This indicates that the macroscopic strain mainly occurs by preffered plastic deformation in the Y-TZP grains. In contrast, the alumina grains were dislocation-free but often contained polyhedral-shape pores within the grains (Fig. 7a). These pores may originate due to accumulation of the vacancy clusters during the plastic deformation or sintering. At similar deformation temperatures, the glass-containing counterpart specimen (Fig. 7b) exhibited Y-TZP grains with round-shape morphologies. These grains were distributed both within the grains and at the grain boundaries of the larger micron-size alumina grains. Nevertheless, the grains of both Y-TZP and alumina were dislocation-free. This confirms the grain boundary sliding to be

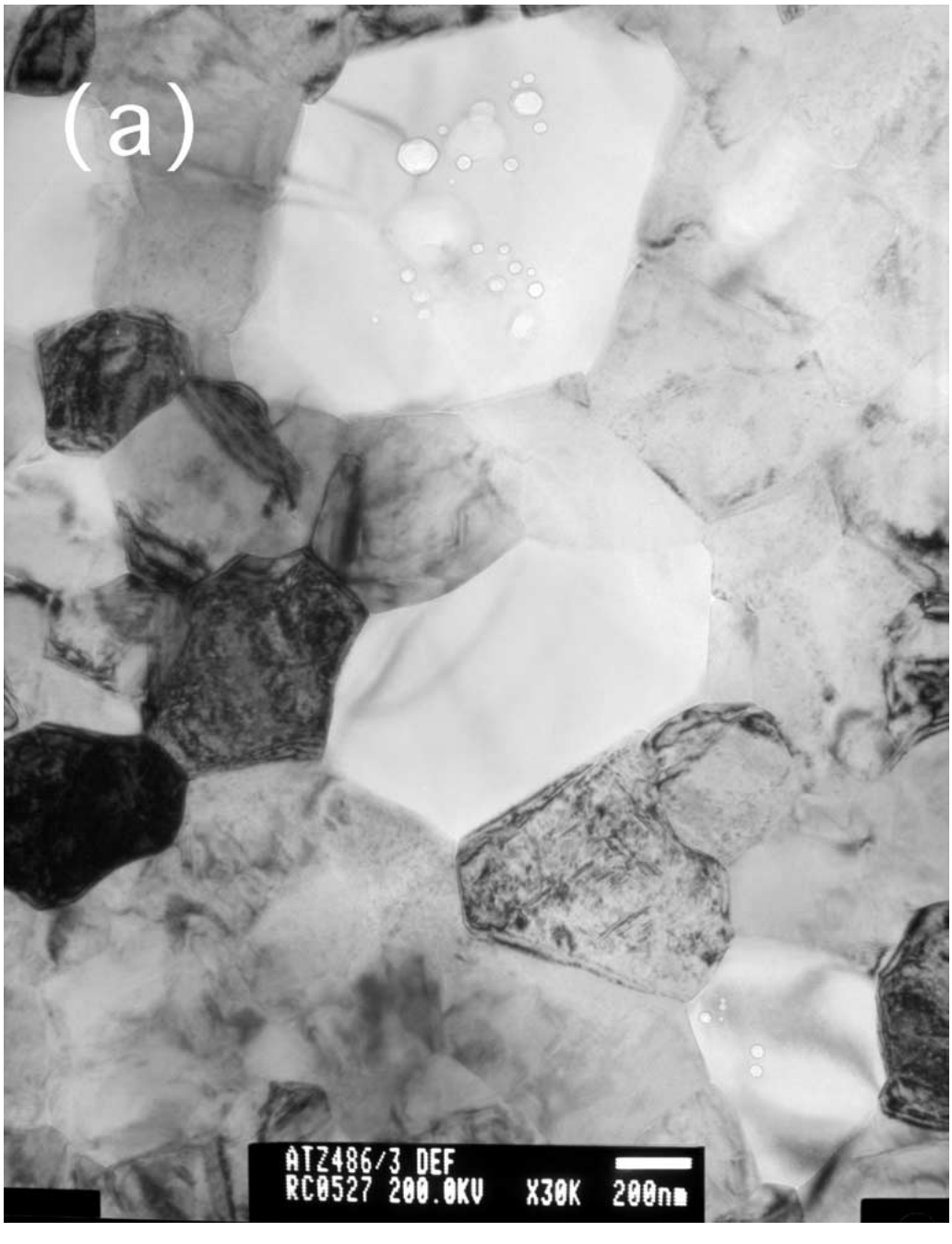

Figure 7 TEM images of specimens deformed at 1375°C: (a) Glass-free ATZ with 58% deformation showing dislocated Y-TZP grains and (b) Glass-containing ATZ with 32% deformation showing the rounded shape of the Y-TZP grains due to the glass. (*Continued*)

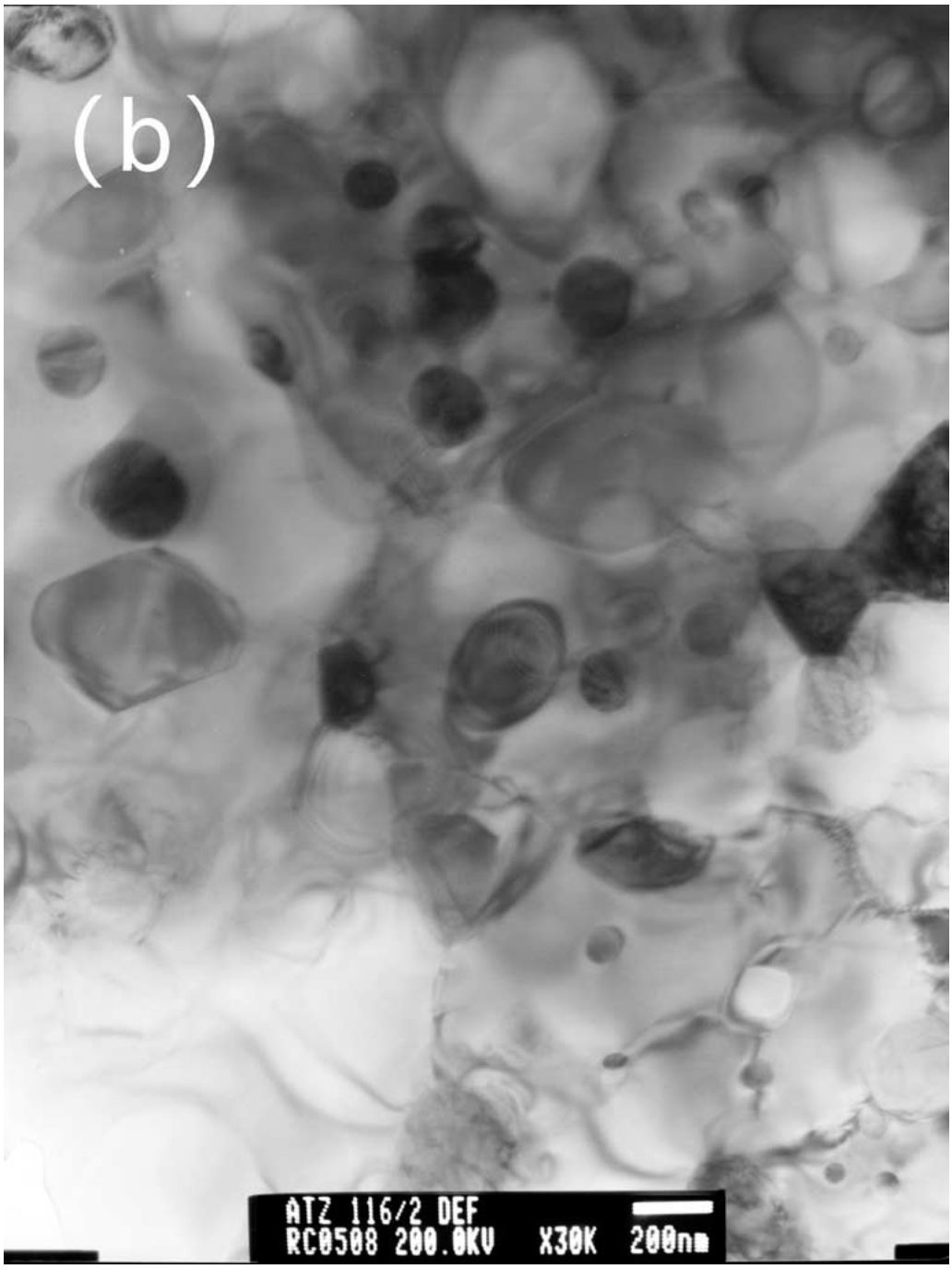

Figure 7 (*Continued*)

a dominant mechanism during the plastic deformation in the glass-containing compositions as opposed to the preffered plastic deformation of the Y-TZP grains in the glass-free specimens.

TEM images from the glass-free specimens, which deformed at different temperatures (i.e., 1400°C in Fig. 8), have shown similar microstructural features. Occasionally, the larger Y-TZP grains consisted of a few finer grains separated by networks of dislocations (low-angle grain boundaries). This may suggest a rotation of the Y-TZP grains as an additional deformation mechanism during the plastic deformation [29]. Such a grain rotation leads to the preffered orientation between the adjacent grains and consequently to the annihilation of the originally high angle grain boundaries. It may result in larger grains by enhanced dynamic grain growth during the plastic deformation.

Considering the overall microstructural changes within the specimens prior to and after the plastic deformation, the deformation behavior may be described as follows: Plastic deformation in glass-free ATZ occurs by grain boundary sliding, where the strains are partially accomodated by intragranular dislocation glide within the zirconia grains. Plastic deformation in the counterpart glass-containing ATZ occurs by viscous flow of the grain boundary glassy phase at lower deformation temperatures and short durations, when the glassy phase retains its amorphous nature. However, this deformation mechanism is lost at higher deformation temperatures and for longer durations, whenever the glass is subjected to crystallization. Consequently, grain boundary sliding similar to that of ATZ alloys are expected at the latter conditions.

Figure 8 TEM image of the glass-free ATZ deformed at 1400°C with 52% deformation. High dislocation density and low-angle grain boundaries are visible within the Y-TZP grains.

4. Summary and conclusions

A fabrication procedure was developed through which near fully dense ATZ and ATZ-Oxynitride glass nanocomposites were formed by MW sintering at low temperature (1380°C). A relatively large amount of oxynitride glass could be added without causing a significant effect on both the densification and the grain growth of the crystalline oxide grains.

Under uniaxial compression conditions, strain rates as high as 10^{-4} (s^{-1}) were recorded at 1350°C. The compressive stress required for obtaining a given strain rate in the glass-free ATZ (i.e., 90 MPa and 10^{-4} (s^{-1}) at 1350°C) was significantly reduced due to the presence of the oxynitride glass (i.e., 40 MPa). The increase in the strain rate is due to cooperative grain boundary sliding, aided by viscous flow of the intergranular glassy phase at 1250°C. The deformation behavior at higher temperatures was related to the simultaneous effect of glass crystallization (in the latter stages of the compression process) and plastic deformation by grain boundary sliding. Dynamic growth of alumina grains was inhibited in the presence of the glass.

Acknowledgements

The authors thank the Israel Ministry of Science for supporting this research through the infrastructure grant #1090-1-98.

References

1. F. WAKAI and H. KATO, *Adv. Ceramic Mater.* **3** (1988) 71.
2. T. G. NIEH, C. M. McNALLY and J. WADSWORTH, *Scr. Metall.* **23** (1989) 457.

3. L. CLARISSE, R. BADDI, A. BATILLE, J. CRAMPON, R. DUCLOS and J. VICENS, *Acta Mater.* **45** (1997) 3843.
4. E. SATO, H. MORIOKA, K. KURIBAYASHI and D. SUNDARARAMAN, *J. Mater. Sci.* **34** (1999) 4511.
5. H. YOSHIDA, K. OKADA, Y. IKUHARA and T. SAKUMA, *Phil. Mag.* **76** (1997) 9.
6. O. FLACHER, J. J. BLANDIN and K. P. PLUCKNETT, *Mater. Sci. Eng.* A **221** (1996) 102.
7. T. TSUKUMA, K. UEDA and M. SHIMADA, *J. Amer. Ceram. Soc.* **68** (1985) C-4.
8. S. RAJENDRAN, M. V. SWAIN and H. J. RUSSELL, *J. Mater. Sci.* **23** (1988) 1805.
9. J. L. SHI, J. H. GAO, B. S. LI and T. S. YEN, *J. Eur. Ceram. Soc.* **15** (1995) 967.
10. T. S. SUZUKI, Y. SAKKA, K. MORITA and K. HIRAGA, *Scr. Mater.* **43** (2000) 705.
11. K. NAKANO, T. S. SUZUKI, K. HIRAGA and Y. SAKKA, *ibid.* **38** (1998) 33.
12. J. FREIM and J. McKITTRICK, *J. Amer. Ceram. Soc.* **81** (1998) 1773.
13. J. G. WANG and R. RAJ, *ibid.* **67** (1984) 399.
14. R. CHAIM, *J. Mater. Res.* **14** (1999) 2508.
15. Y. IKUHARA, P. THAVORNITI and T. SAKUMA, *Mater. Sci. Forum* **243–245** (1997) 345.
16. A. A. SHARIF and M. L. MECARTNEY, *Acta Mater.* **51** (2003) 1633.
17. A. GOLDSTEIN, N. TRAVITZKY, A. SINGURINDY and M. KRAVCHIK, *J. Eur. Ceram. Soc.* **19** (1999) 2067.
18. F. WAKAI, *Brit. Ceram. Trans. J.* **88** (1989) 205.
19. T. G. NIEH, J. WADSWORTH and O. D. SHERBY, "Superplasticity in Metals and Ceramics" (Cambridge Univ. Press, UK, 1997) p. 101.
20. D. M. OWEN and A. H. CHOKSHI, *Scr. Metall.* **29** (1993) 869.
21. J. CHEVALIER, C. OLAGNON, G. FANTOZZI and H. GROS, *J. Eur. Ceram. Soc.* **17** (1997) 859.
22. F. WAKAI, H. KATO, S. SAKAGUCHI and N. MURAYAMA, *J. Ceram. Soc. Jpn.* **94** (1986) 1017.
23. M. JIMENEZ-MELENDO, A. DOMINGUEZ-RODRIGUEZ and A. BRAVO-LEON, *J. Amer. Ceram. Soc.* **81** (1998) 2761.
24. A. H. CHOKSHI and T. G. LANGDON, *Mater. Sci. Tech.* **7** (1991) 577.
25. M. JIMENEZ-MELENDO, A. BRAVO-LEON and A. DOMINGUEZ-RODRIGUEZ, *Mater. Sci. Forum* **243–245** (1997) 363.
26. J. L. SHI, Z. L. LU, J. H. GAO, G. Q. ZHU, L. LI and T. R. LAI, *Acta Mater.* **46** (1998) 1923.
27. K. MORITA and K. HIRAGA, *Acta Mater.* **50** (2002) 1075.
28. B. W. KIBBLE and A. H. HEUER, in "Advances in Ceramics," Science and Technology of Zirconia II, edited by N. Claussen, M. Ruhle and A. H. Heuer (The ACerS Inc., Columbus, Ohio, 1984) Vol. 12, p. 415.
29. R. CHAIM, R. RAMAMOORTHY, A. GOLDSTEIN, I. ELDROR and A. GURMAN, *J. Eur. Ceram. Soc.* **23** (2003) 647.
30. H. MUTO, T. FUTAMI and M. SAKAI, *J. Mater. Res.* **16** (2001) 1879.
31. H. MUTO and M. SAKAI, *Acta Mater.* **48** (2000) 4161.

Received 19 June 2003
and accepted 25 August 2004